EIGHTEENTH EUROPEAN ROTORCRAFT FORUM

A - 01

Paper No 15

VALIDATION OF THE ROTAC CODE FOR THE ROTOR NOISE PREDICTION

P. GNEMMI, J. HAERTIG, Ch. JOHÉ
ISL, FRANCE

September 15-18, 1992

AVIGNON, FRANCE

ASSOCIATION AERONAUTIQUE ET ASTRONAUTIQUE DE FRANCE

VALIDATION OF THE ROTAC CODE

FOR THE ROTOR NOISE PREDICTION

P. GNEMMI, J. HAERTIG, Ch. JOHÉ

French-German Research Institute
5, rue du Général Cassagnou
68301 SAINT LOUIS (France)

Abstract

The blade/vortex interaction noise and the thickness noise are the impulsive noises radiated by a helicopter rotor flying at low speed. A prediction code of the thickness and loading noises applied to a helicopter rotor has been developed at ISL. This code, named ROTAC, is very briefly described here.

In order to validate this acoustic code, calculations are compared with measurements obtained by ISL and by a DLR US-ARMY collaboration.

The thickness noise of a rotor in hover and forward flight is correctly predicted up to a tip Mach number near 0.88. For a flight configuration with occurrence of blade/vortex interaction, the small number of blade pressure measurements does not allow to determine the amplitude of the loading noise but these entry data make it possible to examine qualitatively the agreement between calculations and measurements.

Notations

- a_0 : sound speed in undisturbed medium
- c : blade chord
- D : rotor diameter
- ℓ_i : surface density of the aerodynamic force acting by the blade element $d\sigma$ on the fluid
- M_{at} : advancing tip Mach number
- M_h : hover tip Mach number
- M_r : Mach number in the receiving direction
- $\tilde{p}$: acoustic pressure
- R : distance between the receiving point and the rotor hub
- R_E : rotor radius (D/2)
- r_i : location vector of the receiving point with respect to the blade element $d\sigma$
- r : distance between the receiving point and the blade element $d\sigma$
- t : noise receiving time
- v_n : normal component of the blade element velocity
- $\vec{x}$: location vector of the receiving point
- α_q : inclination angle of the rotor disk
- Θ : azimuth angle of the receiving point with respect to the rotor hub
- θ : blade pitch angle
- θ_0 : collective blade pitch angle (at 0,75 R_E or at 0,70 R_E)
- θ_{ic} : lateral cyclic pitch angle term
- θ_{is} : longitudinal cyclic pitch angle term
- μ : rotor advance ratio
- ρ_0 : air density
- $d\sigma$: blade element surface
- τ : noise emission time
- Φ : sight angle of the receiving point with respect to the rotor hub
- ψ : blade azimuth angle
- Ω : rotor blade angular velocity.

Introduction

The impulsive noises radiated by a helicopter rotor are the blade/vortex interaction noise which is very important at low speed in descent flight, the quadrupolar noise which occurs at high speed and the thickness noise occurring in all cases.

We have developed a prediction code of the thickness and loading noises (ROTAC) which

computes in time domain and is suitable for subsonic speeds and non-compact sources.

In this presentation we are particularly interested in validating the acoustic code ROTAC by comparing the calculated results with the experimental ones obtained by ISL (thickness noise in hover flight) and by the DLR US-ARMY collaboration (thickness and loading noises in forward flight).

The pressure measurements given by several sensors located on the blade are used as entry data for the loading noise calculation.

1 The acoustic code ROTAC

The theoretical study of the noise radiated by bodies moving with respect to the air is based on a non-homogeneous wave equation, several source terms of the second member indicating the boundary conditions on the body surfaces. The resolution of this equation (called Ffowcs-Williams and Hawkings equation) leads to the expression of the radiated acoustic pressure. Neglecting the influence of the quadrupolar noise, one obtains the full formulation of the thickness and loading noises, respectively [1,2,3] :

$$4\pi\,\tilde{p}(\vec{x},t) = \int_S \left\{ \frac{\rho_0}{r(1-M_r)^2}\left[\frac{\partial v_n}{\partial \tau} + \frac{v_n}{1-M_r}\left(\frac{r_j}{r}\frac{\partial M_j}{\partial \tau} + \frac{a_0}{r}\left(M_r - M_j^2\right)\right)\right] d\sigma \right\}_{\tau=\tau_e}$$

$$+ \int_S \left\{ \frac{1}{a_0\, r(1-M_r)^2}\left[\frac{r_i}{r}\frac{\partial \ell_i}{\partial \tau} + \frac{1}{1-M_r}\left(\frac{\ell_i\, r_i}{r}\right)\left(\frac{r_j}{r}\frac{\partial M_j}{\partial \tau}\right)\right] \right.$$

$$\left. + \frac{1}{r^2(1-M_r)^2}\left[\left(\frac{\ell_i\, r_i}{r}\right)\left(\frac{1-M_j^2}{1-M_r}\right) - \ell_i\, M_i \right] \right\}_{\tau=\tau_e} d\sigma \,. \qquad (1)$$

The far-field approximation is obtained when the $1/r^2$ terms in the above full formulation are neglected.

The acoustic calculation code, named ROTAC, is based on a temporal formulation similar to the one developed by FARASSAT and SUCCI [1] or BRENTNER [4]. This code has been operative since 1989 and has been applied to helicopter rotor prediction noise.

The code is largely described in [2,3,5]; nevertheless, some clauses relative to the different angles may be worth remembering:

- the blade azimuth angle ψ is zero when the blade is located at the back of the rotor,
- the location of the receiving point defined by $\vec{x}$ is given in spherical coordinates by Θ, Φ and R,
- the Θ angle is the location of the azimuthal receiving point with respect to the rotor hub; it is positive in the rotor rotational direction (the rotor turning counter-clockwise) and it is zero when the receiving point is ahead of the rotor.
- Φ is the sight angle of the receiving point with respect to the rotor hub; it is negative when the point is below the horizontal plane and it is zero when the receiving point is in this plane,
- finally, R is the distance between the rotor hub and the receiving point.

The knowledge of the geometry and the kinematics of the rotor is strictly necessary for the calculation of the radiated noise. Further, the knowledge of the aerodynamic forces acting on the blades is necessary for the loading noise calculation.

The validation of the acoustic code ROTAC is made by comparing the calculated results with the experimental ones, the flight conditions being well known. The selected procedure for these comparisons is carried out at three levels:

- validation of the calculated thickness noise for a rotor in hover flight,
- validation of the calculated thickness noise for a rotor in forward flight,
- validation of the calculated loading noise for a rotor in forward flight.

When the noise radiated by a rotor is examined, the calculated thickness noise can be distinguished from the calculated loading noise. But experimentally, it is impossible to dissociate these two kinds of noises, even if their directivities radiate differently. Therefore, for the loading noise validation, we also calculate the thickness noise.

2 Thickness noise of a rotor in hover flight

To validate the thickness noise calculation in the hovering case, we compare the ROTAC results with the acoustic measurements obtained with the ISL rotor model.

2.1 ISL rotor model

This experimental apparatus operating in the open air allows to reach transonic speeds at the rotor blade tips.

This equipment is original because for transonic speeds, the power available at the rotor head and necessary to overcome the drag force is such that the rotor head can be equipped with large chord blades, the chord dimension being two or four times smaller than the chord of real size helicopter rotor blades.

The facility, the control and the data acquisition system are described in [6].

The general characteristics of this rotor model are the following:

- power at the rotor head : 140 kW
- maximal speed of the rotor head : 3000 rev/min
- maximal torque : 467 Nm
- height with respect to the ground : 2,50 m
- rotation direction seen from above : clockwise.

The characteristics of the actually used blades are as follows:

- rotor diameter : 2,00 m
- blade root radius : 0,28 m
- profile kind : NACA0012
- profile chord : 0,15 m
- linear twist : + 6,945 °/m
- blade mass : 1,400 kg
- blade number : 2.

2.2 Acoustic recordings

The purpose of the experiments consists in recording the acoustic signatures at the receiving points located around the rotor for rotation speeds ranging from 1900 rev/min to 3000 rev/min, the blade tip pitch angle being zero.

For a given rotation velocity, a synchronous data acquisition is triggered when the reference blade is seen by the camera located $\pi/2$ ahead of the receiving points (figure 1). The maximum acquisition rate is 280 kHz. A test record consists of 16 revolutions and 1024 samples are recorded per revolution. The measured signatures are obtained by making the phase average over the 16 revolutions. We only present the signatures of two microphones among the five ones used in this experiment:

- microphone M01 is located in the horizontal plane one diameter from the rotor hub ($\Phi = 0, R = D$),
- microphone M02 is located 20° below the horizontal plane one diameter from the rotor hub ($\Phi = -20°, R = D$).

The ground below the rotor was covered with acoustic lining to avoid reflections.

2.3 ROTAC thickness noise calculation

We use the ROTAC code to compute the acoustic signatures at the location of the microphones with a time step corresponding to the experimental sampling rate (1024 samples per revolution). The ROTAC code input data are the same as the experimental conditions. In order to respect the propagation delay, the computation is started at an azimuth angle corresponding to the triggering of the data acquisition.

2.4 Comparison between computed and experimental results

Figure 2 shows results concerning microphone M01 (horizontal plane) with $M_h = 0.85$:

- the measured signature,
- the computed signature using the full formulation (equation 1),
- the computed signature using the far-field approximation.

The computed signature using the full formulation has the same shape as the measured one but the noise is underestimated about 13%. As regards the far-field approximation, the prediction is roughly 30% smaller than the measurement and a time delay is noted. As an example, this case demonstrates that the full formulation (equation 1) is necessary to predict the noise radiated at distances in the order of the rotor diameter.

At the same location (microphone M01, $\Phi = 0$, $R = D$) the predicted and measured signatures obtained for six hovering tip Mach numbers ($0.65 \leq M_h \leq 0.89$) are presented in figure 3, the time scale corresponding to about 1/5 of a revolution. A good agreement is found especially for the shape of the signature but the level is underestimated; the deviation is less than 10% at $M_h = 0.65$ and less than 20% at $M_h = 0.89$.

Figure 4 presents the same kind of comparison for microphone M02 ($\Phi = -20°$, $R = D$). The pressure scale is twice as low as in the above case (microphone M01) and so is the noise level. A good agreement is found again, the deviation between predicted and measured levels is lower than 15%.

3 Thickness noise in forward flight

We have compared the predicted signatures given by the ROTAC code with measurements obtained with an AH-1/OLS model rotor at the DNW wind tunnel and with flight tests. These tests were performed thanks to the collaboration between the DLR and the US-ARMY in 1982 [7].

Figure 5 presents the variation of the pressure level of the thickness noise negative peak versus the advancing tip Mach number (M_{at}) measured and computed at 1.8 diameter ahead of the rotor in the horizontal plane ($\Theta = 0$, $\Phi = 0$, $R = 1.8D$).

In spite of a little overprediction concerning the calculated thickness noise with the far-field approximation at low Mach numbers ($M_{at} < 0.86$), a good agreement is found for the full formulation up to $M_{at} = 0.88$. The small discrepancies between predictions and in-flight measurements may be due to the unknown rotor inclination during the flight tests which is not taken into account.

4 Loading noise in forward flight

Thanks to our collaboration with ONERA, we can use blade pressure measurements and acoustic data obtained by the US-ARMY for the same AH-1/OLS model rotor [8,9,10].

The flight conditions are:

- horizontal wind direction,
- hover tip Mach number $M_h = 0.6647$,
- rotor advance ratio $\mu = 0.1632$,
- rotor disk inclination $\alpha_q = 1°$,
- collective pitch $\theta_0 = 5.31°$,
- cyclic pitch $\theta_{1c} = -1.87°$, $\theta_{1s} = 1.86°$, with the law $\theta = \theta_0 - \theta_{1c} \cos\psi - \theta_{1s} \sin\psi$,
- sound speed $a_0 = 338.61$ m/s,
- air density $\rho_0 = 1.253$ kg/m^3.

- thrust coefficient $C_T = 0.535\ 10^{-2}$.

4.1 Calculation and comparison with experiment

We use the differential pressures measured at 8 stations distributed on the span at 3% chord from the blade leading edge additionally with 3 stations distributed on a chord located at 95.5% from the rotor hub. Then we compute the loading noise radiated by these aerodynamic loads.

Figure 6a shows the temporal evolution of the differential pressures measured at 3% from the leading edge, from the middle of the blade to its tip. Figure 6b shows the time derivative evolution of these pressures.

We also get four acoustic signatures measured at a distance R equal to 1.72 rotor diameter. The location in the wind tunnel of these four microphones is given below:

- microphone M02: in the horizontal plane, ahead of the rotor, $\Theta = 0°$, $\Phi = 0°$
- microphone M03: below the rotor plane, ahead of the rotor, $\Theta = 0°$, $\Phi = -30°$
- microphone M07: below the rotor plane, on the advancing side of the rotor, $\Theta = -30°$, $\Phi = -30°$
- microphone M09: below the rotor plane, on the retreating side of the rotor, $\Theta = -30°$, $\Phi = -30°$.

The noise is computed with a time step corresponding to the experimental sampling rate (1024 samples per revolution) to obtain the same time resolution with regard to the measurements.

Figure 7 shows the measured acoustic signature during one revolution. On the retreating side (microphone M09), we note that the level of the positive peaks is twice as important as the level of the positive peaks on the advancing side (microphone M07).

Figure 8 presents the loading noise signatures calculated with the full formulation (equation 1) at the four microphone stations. The signatures are to be compared with the experimental results in figure 7. The ordinate scales of the measured signatures are twice as large as the ordinate scales of the calculated signatures.

We verify that the shapes of the calculated loading noise are correctly reproduced. With regard to the levels, we can make the following remarks:

- M02: the predicted positive peaks level is four times as low as the measured one, the phase between the two positive peaks is respected.
- M03: the predicted positive peaks level is twice as low as the measured one, the phase between the two positive peaks is also recovered.
- M07: the predicted negative level is in the same order as the measured one.
- M09: the predicted positive peaks level is between two and three times as low as the measured one, the phase between the two positive peaks is recovered again.

The loading noise calculated at the M07 microphone is the worst predicted one. This receiving point is located at about $\pi/2$ ahead of the strong blade/vortex interaction zone on the advancing side ($\psi = 60°$, see figures 6b and 9b presented later). All blade elementary noises received in phase at this M07 microphone contain blade/vortex interaction noise. Thus, in the calculation the integration effect of all elementary noises (radiated by all blade elements) is the most sensitive to the lack of pressure measurements.

4.2 Blade/vortex interaction location

For each signature, we note the receiving time of different acoustic pressure peaks. We consider three positive peaks and one negative peak noticed on three signatures. Figure 9a shows the four considered peaks of one of the signatures.

For each receiving time and for each blade element we determine the noise emission time (which defines the acoustic blade) in order to locate the impulsive noise sources on the rotor disk. Figure 9b shows the positions for which we notice important pressure peaks on the calculated acoustic signatures.

- The first positive peak, marked 1, whose level is low as compared with the most important peak, indicates a blade/vortex interaction near $\psi = 45°$ on the rotor advancing side. Examining figure 6b (time derivatives of the measured differential pressures), we notice this interaction near the middle of the blade.
- The most important peak, marked 2, indicates a strong blade/vortex interaction on the advancing side. This interaction is located between $\psi = 55°$ at the blade tip and $\psi = 75°$ near the middle of the blade. We also recognize this interaction on figure 6b.
- The third peak, marked 3, whose level is twice as low as the second peak, indicates a blade/vortex interaction which occurs on the advancing side near $\psi = 80°$. This peak receiving time is difficult to define because its duration is important as compared with the second peak receiving time. On figure 6b we can see a blade/vortex interaction near $\psi = 80°$ at the blade tip.
- The negative peak, marked 4, indicates a blade/vortex interaction on the retreating side which occurs near $\psi = 315°$. This interaction is also recognizable on figure 6b.

For this flight configuration, the maximum of the loading noise is generated by the blade/vortex interaction which occurs on the advancing side between $\psi = 55°$ at the blade tip and $\psi = 75°$ near the middle of the blade.

These results do not enable us to conclude on the total validity of the calculated loading noise, owing to the small number of embarked transducers.

4.3 Estimation of the total noise

The thickness noise is also computed with the full formulation (equation 1) for the complete blade. Figure 10 shows the calculated thickness noise for the same microphones. We compare this signatures with the measured ones (figure 7). We note a good agreement between the calculation and the measurement for the M02 microphone. For the other microphones, we cannot reach conclusions because we are unable to distinguish the measured thickness noise from the measured loading noise.

In order to examine the phase deviations between the calculated loading noise and the calculated thickness noise, we use an 'artifice'; this consists in applying a multiplying coefficient to each calculated noise signature of figure 8 to re-establish this loading noise at a comparable level to the measured one (multiplying coefficient 4 for M02, 2 for M03, 1 for M07 and 3 for M09). Now, we add the precedent calculated thickness noise to this extrapolated loading noise for each receiving point.

These total acoustic signatures are a little spurious, due to high frequencies in the differential pressure measurements. A smoothing of these signatures avoids this inconvenience. Figure 11 shows the acoustic signatures smoothed by a third degree polynomial determined on five points.

Although this kind of 'extrapolation' is not so satisfactory, we note a pretty good agreement between extrapolated results and measurements. From the measured signature obtained on M02 microphone (figure 7), on the one hand, and from the extrapolated signature (figure 11), on the other hand, we determine the receiving time difference between the most important blade/vortex interaction positive peak and the thickness noise negative peak; there is no phase lag between the computation and the measurements.

5 Conclusion

For all the flight cases presented here, the thickness noise calculation with the full formulation gives better results than the far-field approximation. For the rotor in hover flight and in forward flight, the thickness noise prediction is in good agreement with experimental results up to a tip Mach number equal to 0.88.

The small number of surface pressure transducer records (used as input data for the loading noise calculation) do not allow us to conclude on the total validity of the loading noise prediction.

It is fastidious to extrapolate to an entire blade the loading noise computed with aerodynamic loads obtained by a small number of pressure measurements. Although it is not satisfactory, the considered extrapolation used to determine the total loading noise added to the thickness noise calculation (for the entire blade) allows to find a good agreement between the calculated signature shapes and the experiments.

We can hope that this acoustic code, coupled with an efficient aerodynamic code giving the instantaneous loads on a rotor, will supply a complete prediction of the noise radiated by a rotor flying at low speed.

As an example, figure 12 presents the prediction of the thickness and loading noises radiated by the same model rotor AH-1/OLS for the same configuration studied at paragraph 4. The aerodynamic loads are computed with the ROTAR code also developed at ISL; these aerodynamic results are published in [11].

Bibliography

1. FARASSAT F. and SUCCI G. P., The prediction of helicopter rotor discrete frequency noise, Vertica, Vol. 7, No 4, pp. 309-320, 1983, 38th Annual Forum, American Helicopter Society, Anaheim/CA, USA, May 4-7, 1982

2. HAERTIG J. et GNEMMI P., Calcul du bruit d'épaisseur et du bruit de charge rayonnés par un rotor en vol d'avancement, ISL - R119/89, 1989

3. GNEMMI P., Thesis to be published

4. BRENTNER K. S., Prediction of helicopter rotor discrete frequency noise, A computer program incorporating realistic blade motions and advanced acoustic formulation, NASA Technical Memorandum 87721, October 1986

5. GNEMMI P., HAERTIG J., JOHÉ Ch. et SCHAFFAR M., Etude de l'interaction pale/tourbillon: acoustique, aérodynamique, modélisations, ISL - R104/92, 1992

6. JOHÉ Ch., HAERTIG J., GNEMMI P. et VINCENT F., Le banc rotor de l'ISL, ISL - R108/92, 1992

7. SCHMITZ F.H., BOXWELL D.A., SPLETTSTOESSER W.R. and SCHULTZ K.J., Model-Rotor High-Speed Impulsive Noise: Full-Scale Comparisons and Parametric Variations, Vertica, Vol. 8, No 4, pp. 395 to 422, 1984

8. BOXWELL D.A., SCHMITZ F.S., SPLETTSTOESSER W.R. and SCHULTZ K.J., Model Helicopter Rotor High-Speed Impulsive Noise: Measured Acoustic and Blade Pressures, presented at the 9th European Rotorcraft Forum, Stresa, Italy, September 1983

9. SPLETTSTOESSER W.R., SCHULTZ K.J., BOXWELL D.A. and SCHMITZ F.S., Helicopter Model Rotor-Blade Vortex Interaction Impulsive Noise: Scalability and Parametric Variations, NASA Technical Memorandum 86007, December 1984

10. SCHULTZ K.J. and SPLETTSTOESSER W.R., Measured and Predicted Impulsive Noise Directivity Characteristics, presented at the 13th European Rotorcraft Forum, Arles, France, September 1987

11. SCHAFFAR M. et HAERTIG J., Computation of the Loads on the AH-1/OLS Model Rotor in Forward Flight and Comparison with Wind Tunnel Tests, presented at the 18th European Rotorcraft Forum, Avignon, France, September 1992

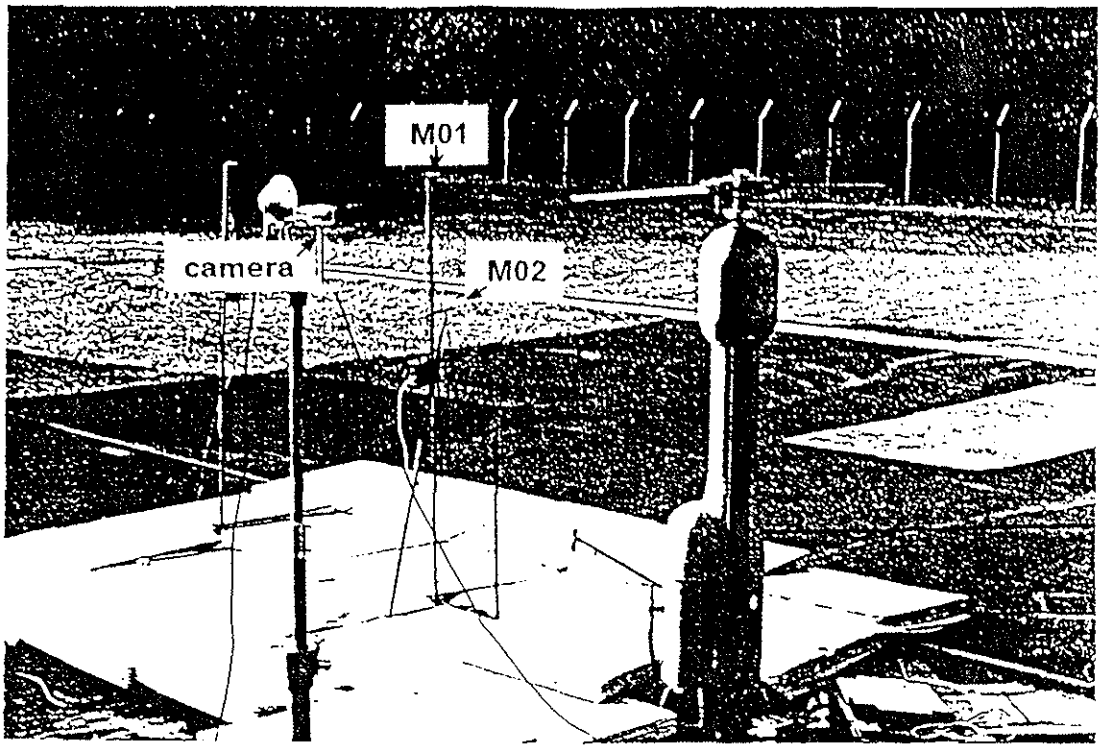

Fig. 1: Microphones location around the ISL model rotor.

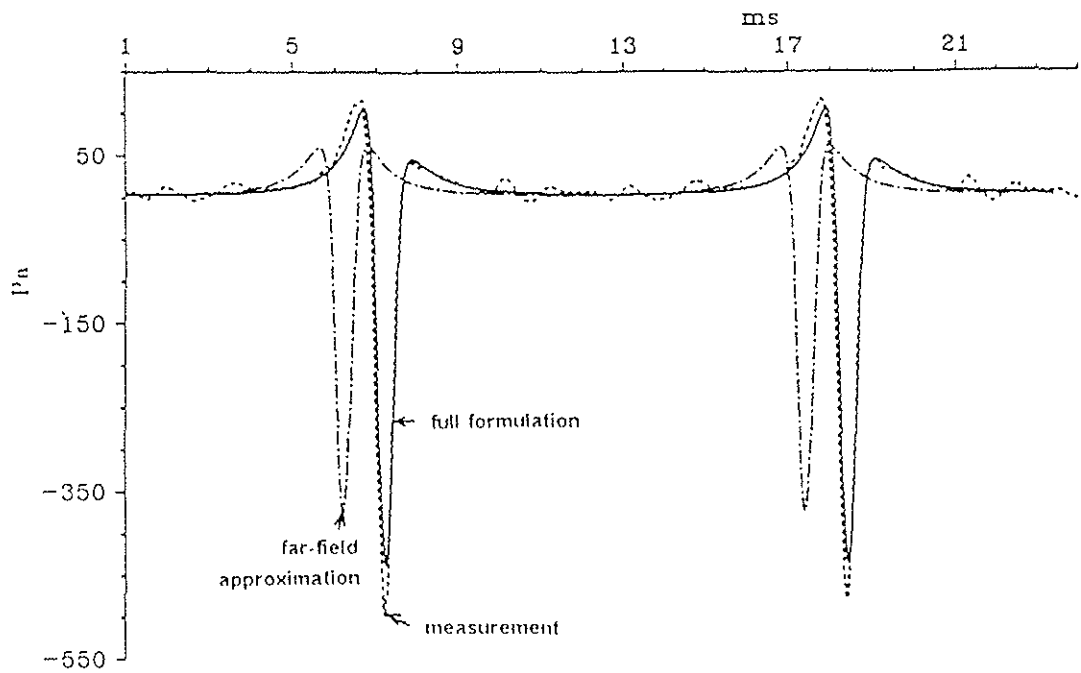

Fig. 2: Comparison of thickness noise calculations with experimental result for the M01 in-plane microphone (ISL rotor in hover flight, $M_{tip} = 0.85$).

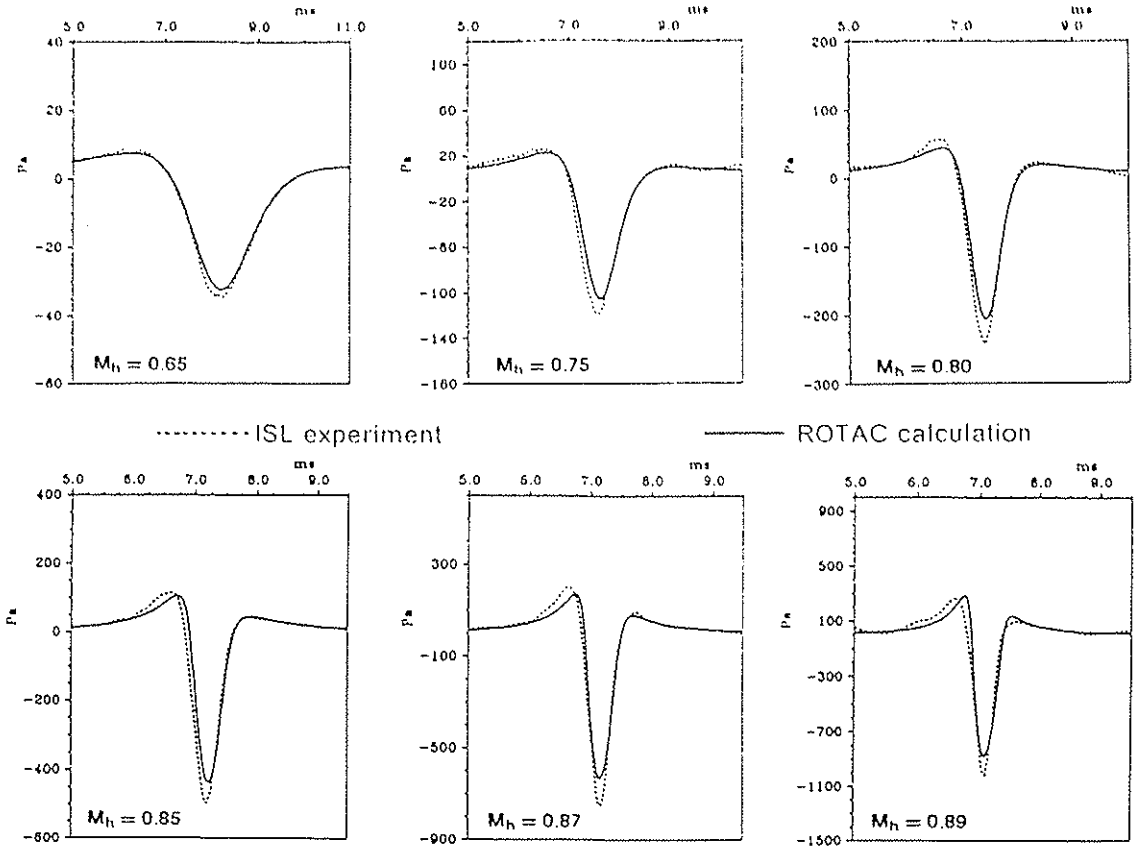

Fig. 3: Comparison of thickness noise calculations with experimental results for the M01 in-plane microphone (ISL rotor in hover flight).

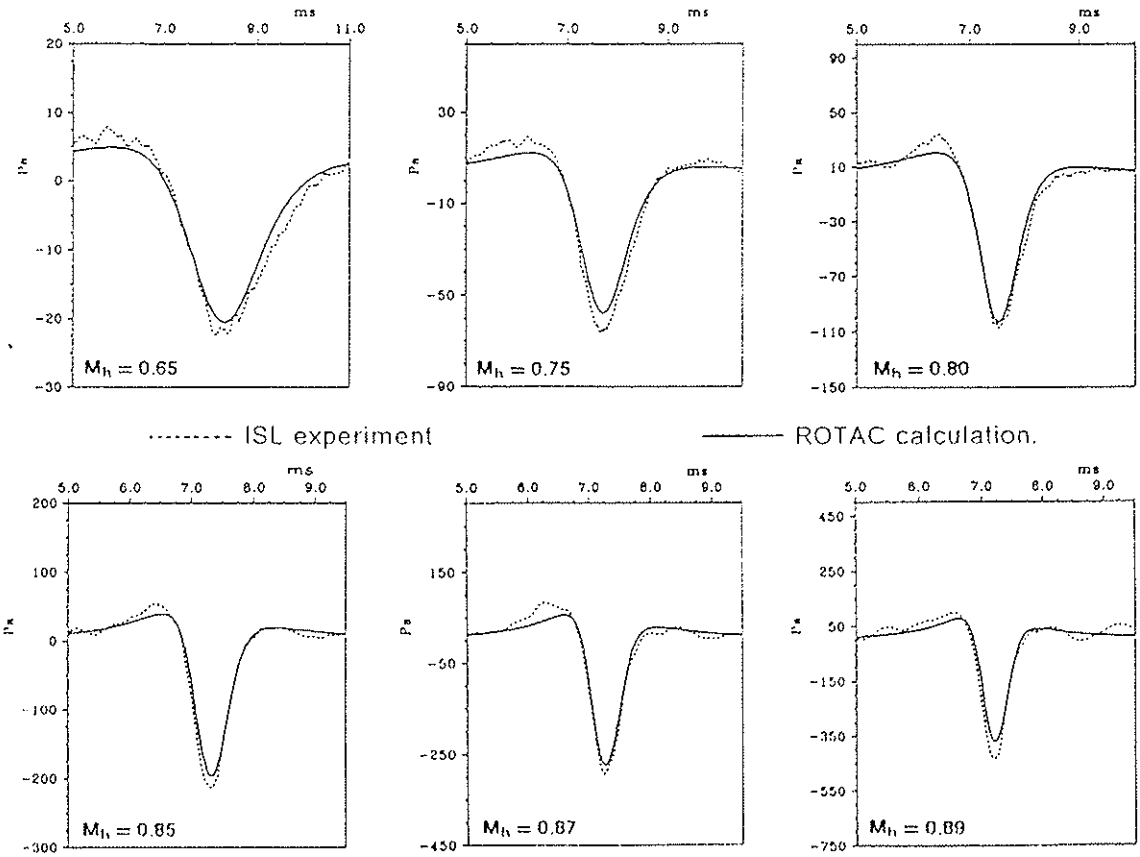

Fig. 4: Comparison of thickness noise calculations with experimental results for the M02 microphone (ISL rotor in hover flight).

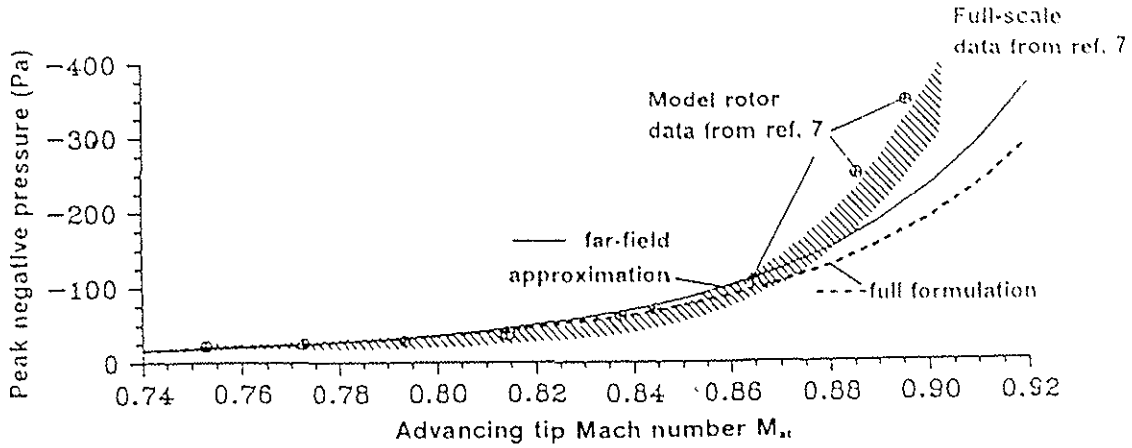

Fig. 5: Comparison of thickness noise calculations with experimental results for an in-plane microphone, 1.8 rotor diameter ahead of the rotor (AH-1/OLS rotor in forward flight).

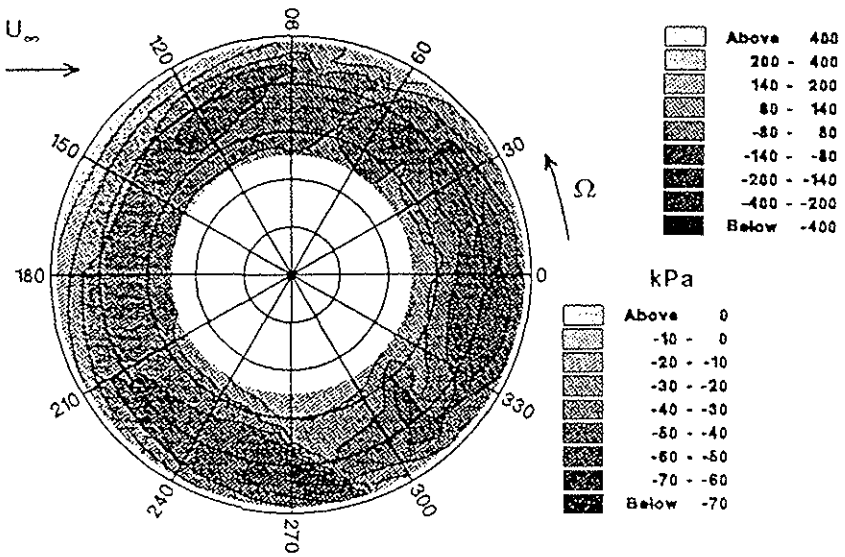

Fig. 6a: Differential pressures measured by 8 transducers located on the chord at 3% from the blade leading edge.

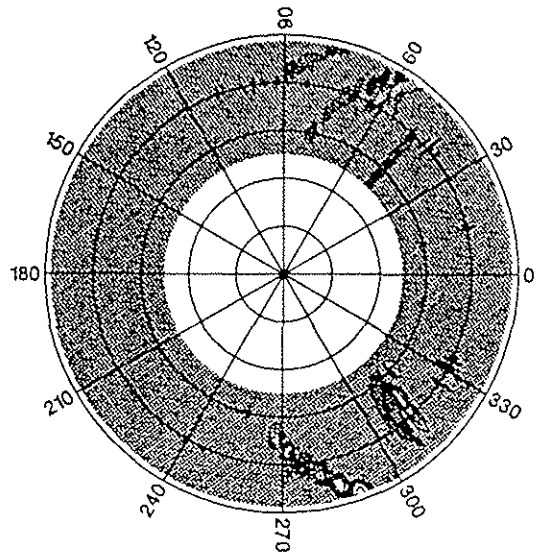

Fig. 6b: Time derivatives of the differential pressures.

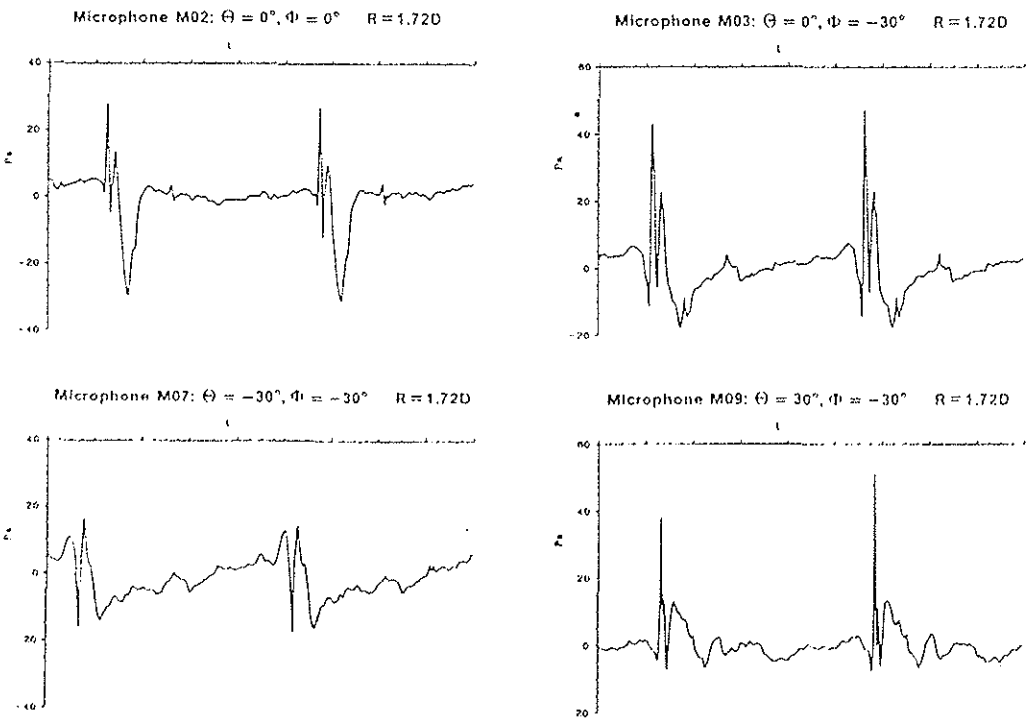

Fig. 7: Measured acoustic signatures at DNW (AH-1/OLS rotor in forward flight)

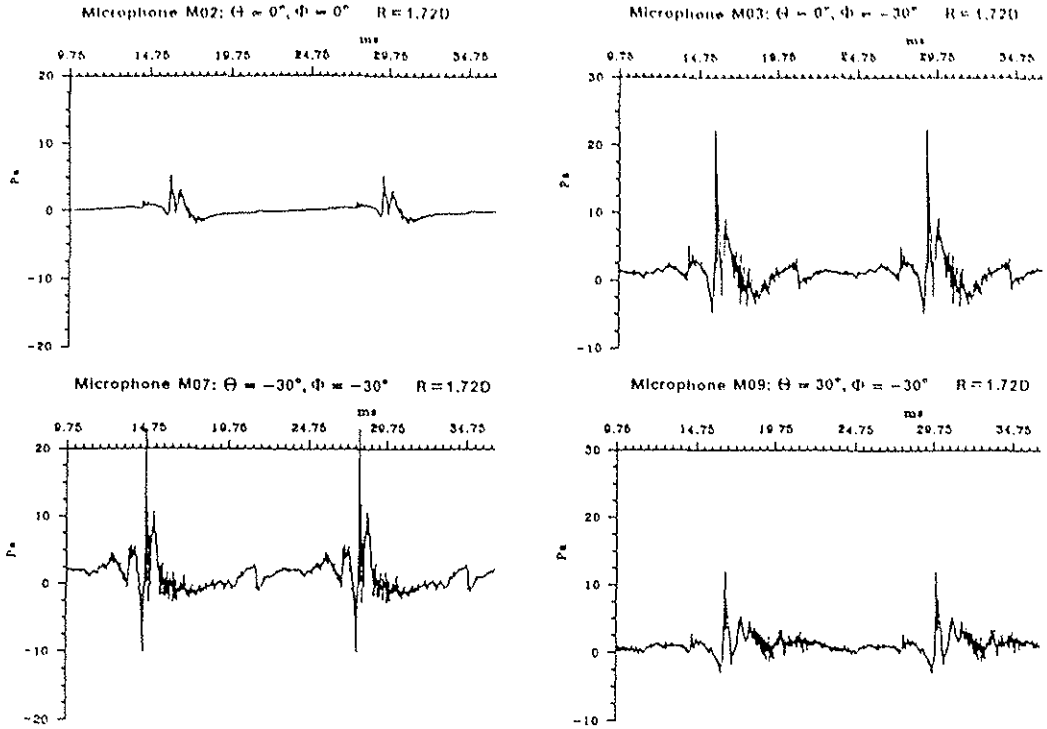

Fig. 8: Calculated loading noise with the differential pressures measured with 11 transducers

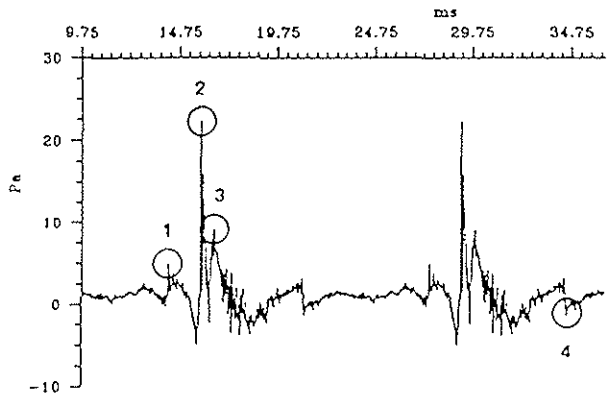

Fig. 9a: Calculated signature (M03), significant peaks for the impulsive noise location.

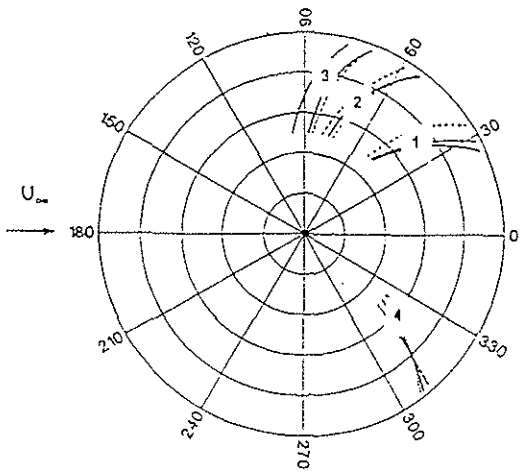

Fig. 9b: Location of the impulsive noise.

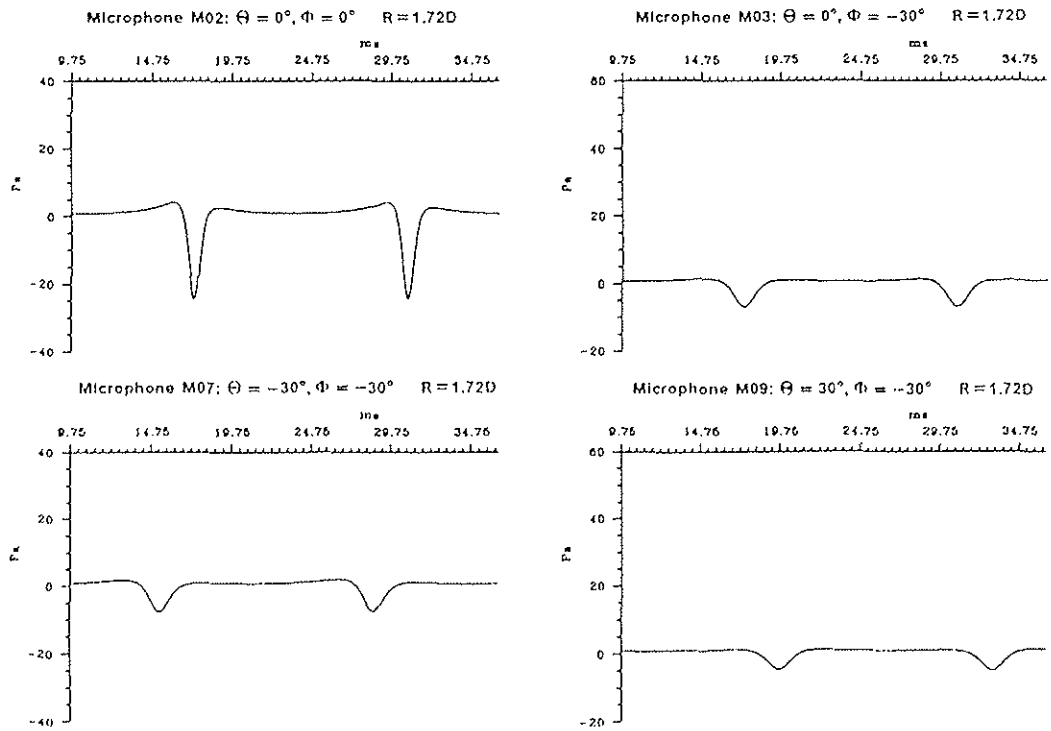

Fig. 10: Calculated thickness noise for the complete blade (AH-1/OLS rotor in forward flight).

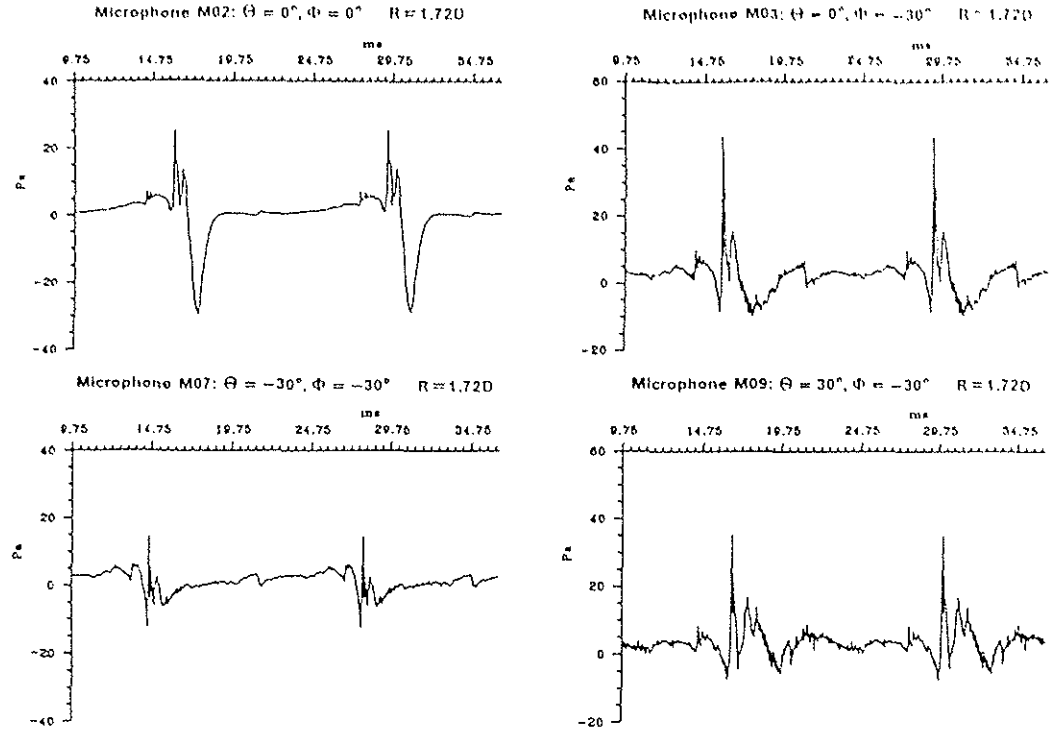

Fig. 11: Calculated total noise: 'extrapolated' loading noise added to thickness noise (to be compared with measurements on figure 7).

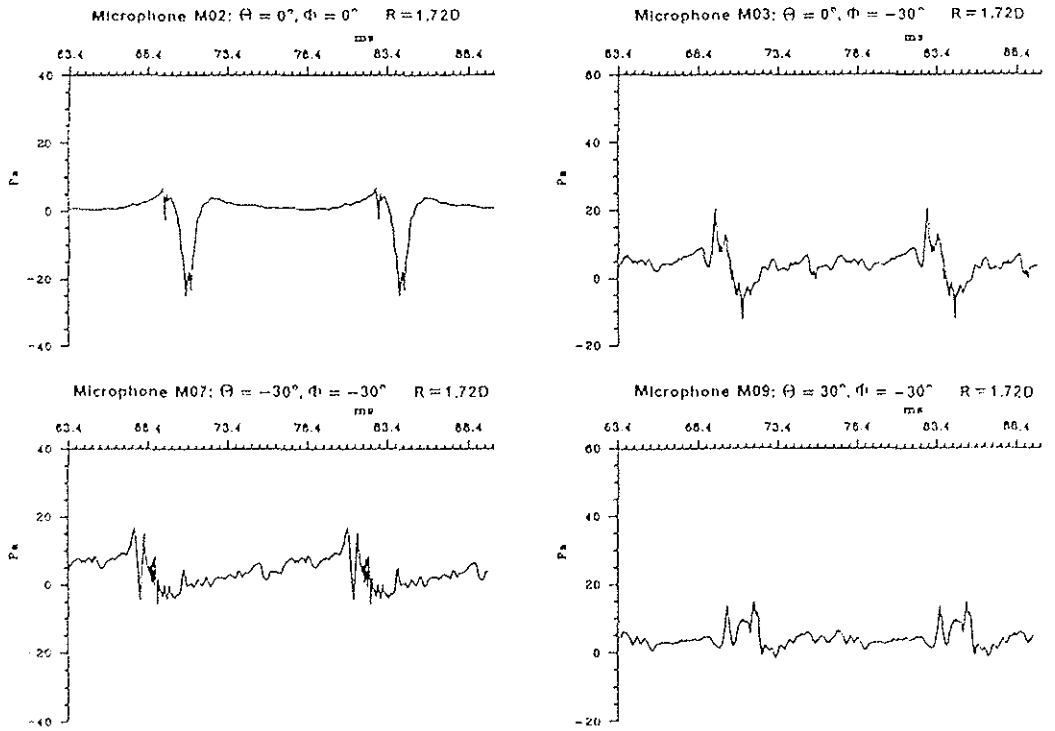

Fig. 12: Calculated loading and thickness noises: the loads are computed with the ROTAR code [13] (to be compared with measurements on figure 7).